Supporting Information

Does Koopmans' Paradigm for 1-Electron Oxidation Always Hold? Breakdown of IP/E_{ox} Relationship for *p*-Hydroquinone Ethers and the Role of Methoxy Group Rotation

*Marat R. Talipov, Anitha Boddeda, Sergey V. Lindeman, Rajendra Rathore**

Department of Chemistry

Marquette University

P.O. Box 1881, Milwaukee, WI 53201-1881

Corresponding Author

*E-mail: rajendra.rathore@marquette.edu

Table of contents

S1. Correspondence between the HOMO shape and CR spin/charge distribution

Table S1. The experimental (X-ray) and calculated [B3LYP/6-31G(d)] bond lengths of the neutral and cation radical of octamethoxydibenzochrysene **DBC** presented in picometers (pm).[1]

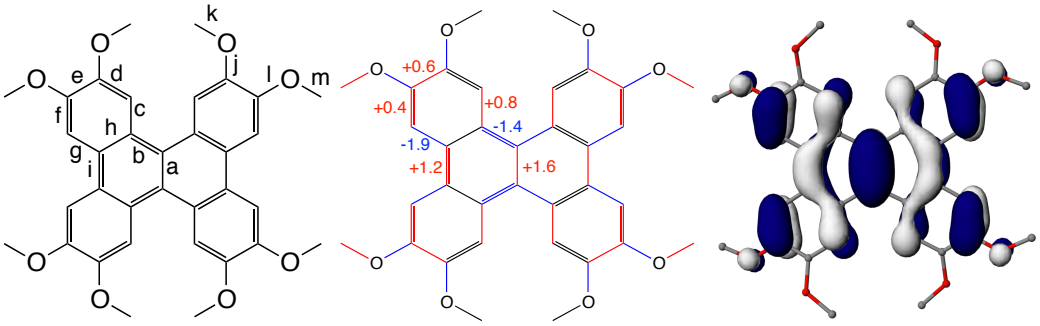

	X-Ray crystallography			B3LYP/6-31G(d)		
Bond[1]	**DBC**	**DBC$^{+\bullet}$**	Δ	**DBC**	**DBC$^{+\bullet}$**	Δ
a	141.4	143.0	**+1.6**	140.3	144.0	+3.7
b	145.5	143.9	**-1.4**	145.8	144.1	-1.7
c	141.5	142.3	**+0.8**	142.2	142.4	+0.2
d	136.9	136.9	**0.0**	138.1	138.0	-0.1
e	141.9	142.5	**+0.6**	142.4	143.0	+0.6
f	137.8	138.2	**+0.4**	138.1	139.3	+1.2
g	142.0	140.1	**-1.9**	141.7	140.4	-1.3
h	141.6	141.6	**0.0**	141.7	142.2	+0.5
i	145.3	146.5	**+1.2**	145.2	146.3	+1.1
j	137.0	135.8	**-1.2**	136.3	135.1	-1.2
k	143.3	143.2	**-0.1**	141.6	142.3	+0.7
l	136.3	134.9	**-1.4**	136.2	134.1	-2.1
m	142.9	144.2	**+1.3**	141.6	142.7	+1.1

[1]Average of equivalent bonds.

Table S2. The experimental (X-ray) and calculated [B3LYP/6-31G(d,p)] bond lengths of the neutral and cation radical of 1,3,6,8-tetraisopropylpyrene **TIP** presented in picometers (pm).[2]

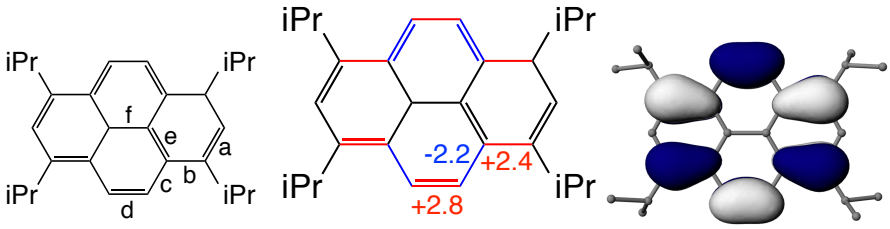

Bond[1]	X-Ray crystallography			B3LYP/6-31G(d,p)		
	TIP	**TIP$^{\bullet+}$**	Δ	**TIP**	**TIP$^{\bullet+}$**	Δ
a	138.9 (3)	138.6 (2)	**-0.3**	139.6	139.5	-0.1
b	141.1 (3)	143.5 (3)	**+2.4**	141.7	144.0	+2.3
c	143.4 (3)	141.2 (3)	**-2.2**	143.5	142.4	-1.1
d	134.7 (3)	137.5 (3)	**+2.8**	135.9	138.0	+2.1
e	142.7 (3)	142.4 (3)	**-0.3**	143.4	143.0	-0.4
f	144.5 (3)	142.7 (4)	**-1.8**	144.0	143.1	-0.9

[1]Average of equivalent bonds.

Table S3. The experimental (X-ray) and calculated [B3LYP/6-31G(d)] bond lengths of the neutral and cation radicals of hexamethoxytriptycene **T3** in picometers (pm).[3]

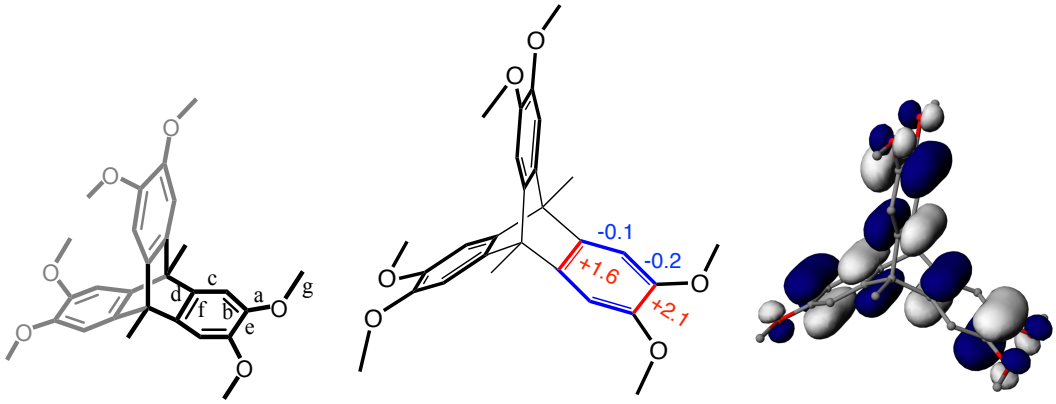

Bond[1]	X-Ray crystallography			B3LYP/6-31G(d)		
	T3	**T3$^{+\bullet}$**	Δ	**T3**	**T3$^{+\bullet}$**	Δ
a	136.6	134.3	**-2.3**	137.2	135.0	-2.2
b	139.8	139.6	**-0.2**	139.2	138.4	-0.8
c	139.6	139.5	**-0.1**	139.0	138.9	-0.1

d	154.2	153.4	**-0.8**	154.0	153.0	-1.0
e	141.3	143.4	**+2.1**	141.1	142.3	+1.2
f	139.6	141.2	**+1.6**	138.8	140.5	+1.7
g	141.5	142.7	**+1.2**	142.7	143.8	+1.1

[1]Average of equivalent bonds.

Table S4. The experimental (X-ray) and calculated [B3LYP/6-31G(d)] bond lengths of the neutral, monomer and dimer cation radicals of octamethylbiphenylene (**OMB**) in picometers (pm).[4]

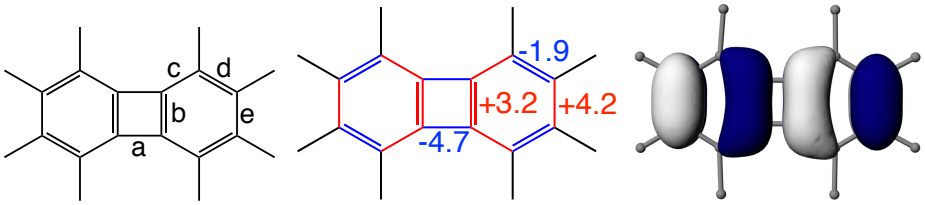

	X-ray crystallography			B3LYP/6-31G(d)		
bond[1]	**OMB**	**$OMB^{+\bullet}$**	**$(OMB)_2^{+\bullet}$**	**OMB**	**$OMB^{+\bullet}$**	**$(OMB)_2^{+\bullet}$**
a	152.2	147.5	149.5	151.6	147.4	149.4
		(-4.7)	**(-2.7)**		**(-4.2)**	**(-2.2)**
b	141.8	145.0	143.2	142.3	144.6	143.4
		(+3.2)	**(+1.4)**		**(+2.3)**	**(+1.1)**
c	136.5	138.6	138.0	137.7	138.6	138.1
		(+2.1)	**(+1.5)**		**(+0.9)**	**(+0.4)**
d	143.5	141.6	142.4	143.7	142.0	142.8
		(-1.9)	**(-1.1)**		**(-1.7)**	**(-0.9)**
e	139.1	143.3	142.0	140.3	143.8	142.0
		(+4.2)	**(+2.9)**		**(+3.5)**	**(+1.7)**

[1]Average of equivalent bonds. [2]Numbers in parenthesis indicate the bond length changes relative to neutral **OMB**.

Table S5. The experimental (X-ray) and calculated [B3LYP/6-31G(d)] bond lengths of the (centrosymmetric) neutral and cation radicals of **BDF1** and **BDF2** in picometers (pm).[5]

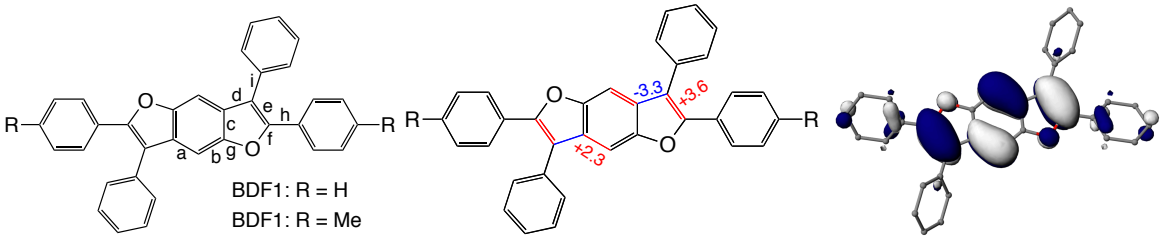

	X-Ray crystallography			B3LYP/6-31G(d)		
Bond[1]	**BDF1**	**BDF1$^{\bullet+}$**	Δ	**BDF1**	**BDF1$^{\bullet+}$**	Δ
a	139.9(1)	142.2(5)	**+2.3**	140.3	141.8	+1.5
b	137.8(1)	135.3(5)	**-2.5**	138.5	137.1	-1.4
c	140.7(1)	142.1(5)	**+1.4**	141.6	142.6	+1.0
d	144.9(1)	141.6(5)	**-3.3**	144.8	142.0	-2.8
e	136.7(1)	140.3(5)	**+3.6**	137.7	141.1	+3.4
f	138.6(1)	136.7(4)	**-1.9**	138.4	136.7	-1.7
g	137.5(1)	137.9(4)	**+0.4**	136.8	137.1	+0.3
h	146.4(1)	144.9(5)	**-1.5**	146.3	144.5	-1.8
i	147.4(1)	147.5(5)	**+0.1**	147.8	147.3	-0.5
	BDF2	**BDF2$^{\bullet+}$**	**Δ**	**BDF2**	**BDF2$^{\bullet+}$**	**Δ**
a	140.0(1)	141.7(2)	**+1.7**	140.3	141.5	+1.2
b	138.1(1)	136.5(2)	**-1.6**	138.5	137.3	-1.2
c	140.9(1)	141.7(2)	**+0.8**	141.5	142.4	+0.9
d	144.7(1)	141.7(2)	**-3.0**	144.8	142.5	-2.3
e	137.1(1)	139.9(2)	**+2.8**	137.7	140.8	+3.1
f	138.6(1)	137.3(2)	**-1.3**	138.5	137.2	-1.3
g	137.3(1)	137.8(2)	**+0.5**	136.9	137.0	+0.1
h	145.9(1)	144.3(2)	**-1.6**	146.1	144.0	-2.1
i	147.8(1)	145.8(2)	**-2.0**	147.7	147.0	-0.7

[1]Average of equivalent bonds.

Table S6. The experimental (X-ray) and calculated [B3LYP/6-31G(d)] bond lengths of the neutral and cation radical of tetramethoxydibenzobicyclo[4.4.1]undecane **BA** presented in picometers.[6]

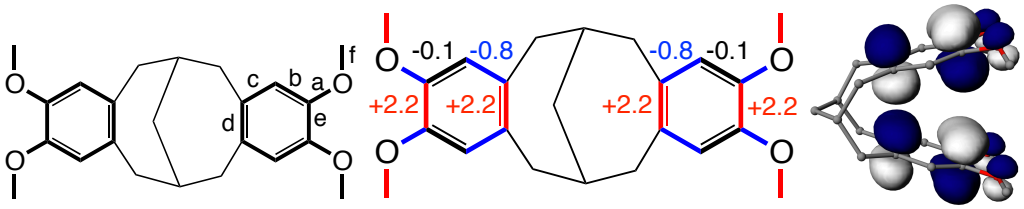

	X-Ray crystallography			B3LYP/6-31G(d)		
Bond[1]	**BA**	**BA**$^{+\bullet}$	Δ	**BA**	**BA**$^{+\bullet}$	Δ
a	137.1	135.4	**-1.7**	136.5	134.5	-2.0
b	138.3	138.2	**-0.1**	139.3	139.7	+0.4
c	140.1	139.3	**-0.8**	140.6	139.6	-1.0
d	139.9	142.1	**+2.2**	140.4	143.1	+2.7
e	140.5	142.7	**+2.2**	141.3	143.5	+2.2
f	142.5	144.1	**+1.6**	141.6	143.7	+2.1

[1]Average of equivalent bonds.

S2. X-ray crystallography data

S2.1. X-ray structure of $^{Me2}HE^{+\bullet}$

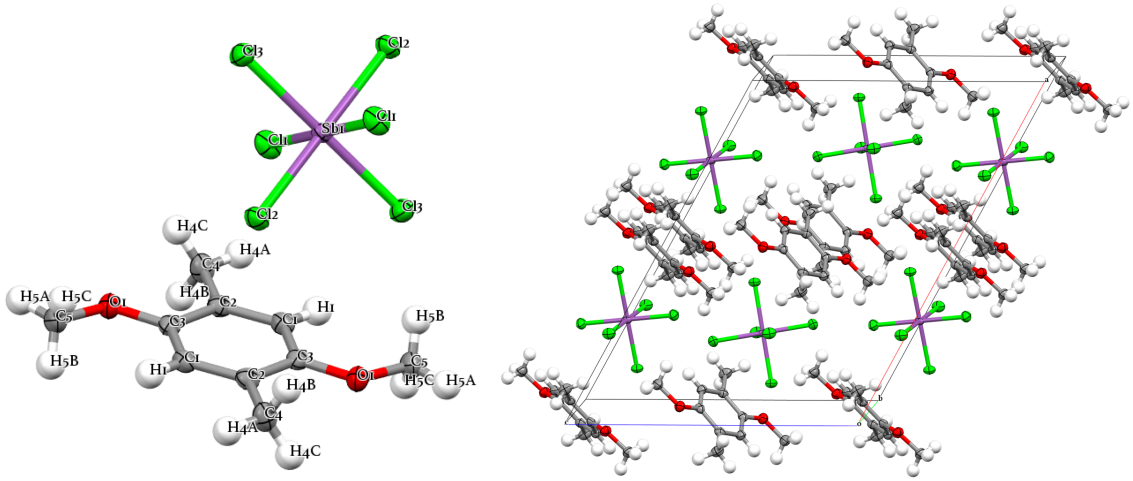

Figure S1. ORTEP and packing diagrams of $^{Me2}HE^{+\bullet}SbCl_6^-$.

Table S7. Crystal data and structure refinement for $^{Me2}HE^{+\bullet}SbCl_6^-$

Identification code	raj7w	
Empirical formula	C10 H14 Cl6 O2 Sb	
Formula weight	500.66	
Temperature	100(2) K	
Wavelength	1.54178 Å	
Crystal system	Monoclinic	
Space group	C 2/c	
Unit cell dimensions	a = 18.5274(4) Å	a= 90°.
	b = 7.7885(2) Å	b= 119.1760(10)°.
	c = 13.6927(3) Å	g = 90°.
Volume	1725.18(7) Å^3	
Z	4	
Density (calculated)	1.928 Mg/m^3	
Absorption coefficient	21.205 mm^{-1}	
F(000)	972	
Crystal size	0.22 x 0.20 x 0.06 mm^3	
Theta range for data collection	5.47 to 66.76°.	
Index ranges	-21<=h<=19, 0<=k<=8, 0<=l<=16	
Reflections collected	6990	
Independent reflections	1426 [R(int) = 0.0269]	
Completeness to theta = 66.76°	98.3 %	
Absorption correction	Numerical	
Max. and min. transmission	0.3627 and 0.0895	
Refinement method	Full-matrix least-squares on F^2	
Data / restraints / parameters	1426 / 0 / 116	
Goodness-of-fit on F^2	1.122	
Final R indices [I>2sigma(I)]	R1 = 0.0200, wR2 = 0.0507	
R indices (all data)	R1 = 0.0209, wR2 = 0.0513	
Largest diff. peak and hole	0.602 and -0.342 e.Å^{-3}	

S2.2. X-ray structure of ^{M}HE

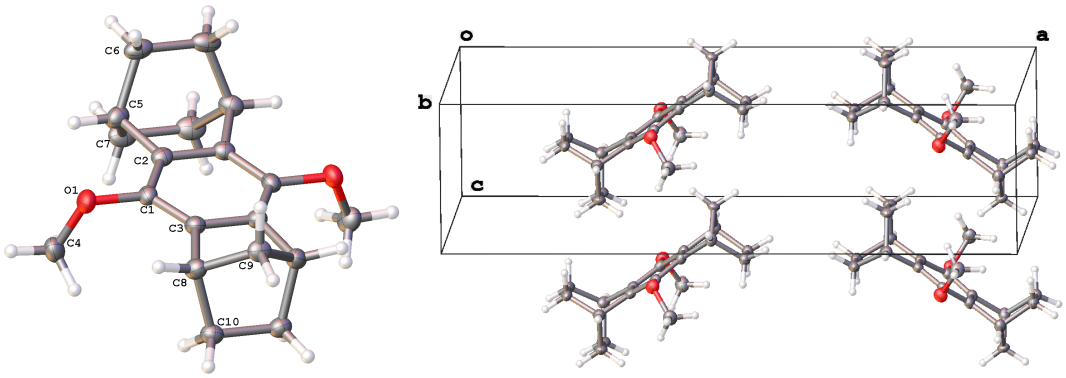

Figure S2. ORTEP and packing diagrams of ^{M}**HE**.

Table S8. Crystal data and structure refinement for ^{M}**HE**

Identification code	raj25h
Empirical formula	$C_{19}H_{23}O_2$
Formula weight	283.37
Temperature/K	100.00(10)
Crystal system	orthorhombic
Space group	Pnma
a/Å	22.1332(4)
b/Å	11.5650(2)
c/Å	5.82560(9)
α/°	90.00
β/°	90.00
γ/°	90.00
Volume/Å^3	1491.18(4)
Z	4
ϱ_{calc}g/cm^3	1.262
μ/mm^{-1}	0.625
F(000)	612.0
Crystal size/mm^3	0.34 × 0.05 × 0.04
Radiation	CuKα (λ = 1.54184)
2Θ range for data collection/°	7.98 to 147.56
Index ranges	-27 ≤ h ≤ 19, -12 ≤ k ≤ 14, -6 ≤ l ≤ 7
Reflections collected	7656
Independent reflections	1575 [R_{int} = 0.0261, R_{sigma} = 0.0158]
Data/restraints/parameters	1575/0/102
Goodness-of-fit on F^2	1.044
Final R indexes [I>=2σ (I)]	R_1 = 0.0496, wR_2 = 0.1376
Final R indexes [all data]	R_1 = 0.0548, wR_2 = 0.1450
Largest diff. peak/hole / e Å^{-3}	0.39/-0.24

S2.3. X-ray structure of $^{M}HE^{+\bullet}$

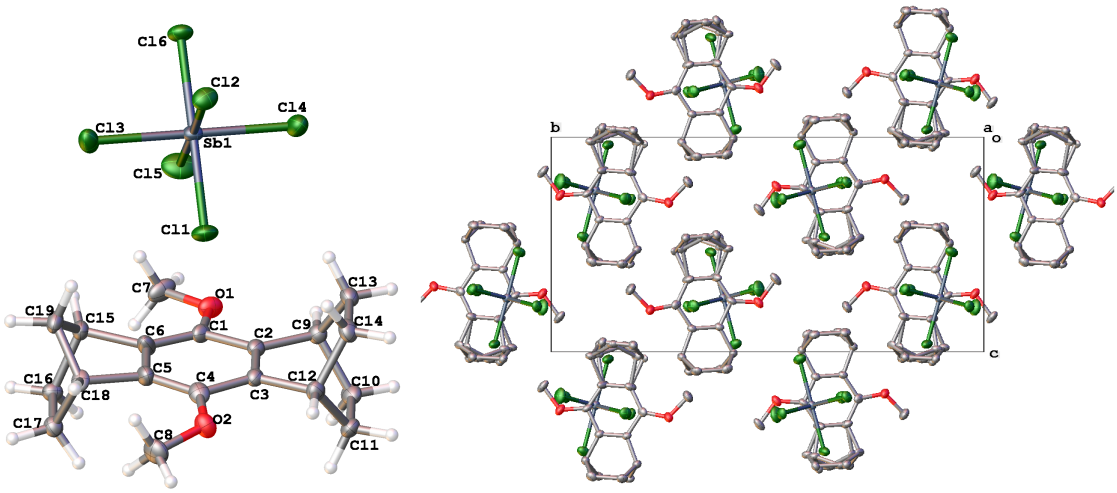

Figure S3. ORTEP and packing diagrams of $^{M}HE^{+\bullet}SbCl_6^-$.

Table S9. Crystal data and structure refinement for $^{M}HE^{+\bullet}SbCl_6^-$.

Identification code	raj25a
Empirical formula	$C_{19}H_{24}O_2Cl_6Sb$
Formula weight	618.83
Temperature/K	100.00(10)
Crystal system	monoclinic
Space group	$P2_1/n$
a/Å	10.07958(17)
b/Å	21.4803(4)
c/Å	10.71257(17)
α/°	90.00
β/°	96.3692(16)
γ/°	90.00
Volume/Å^3	2305.08(7)
Z	4
ϱ_{calc}g/cm^3	1.783
μ/mm^{-1}	16.012
F(000)	1228.0
Crystal size/mm^3	0.413 × 0.0353 × 0.0234
Radiation	CuKα (λ = 1.54184)
2Θ range for data collection/°	8.24 to 148.34
Index ranges	-8 ≤ h ≤ 12, -26 ≤ k ≤ 26, -13 ≤ l ≤ 13
Reflections collected	22323
Independent reflections	4597 [R_{int} = 0.0464, R_{sigma} = 0.0323]
Data/restraints/parameters	4597/10/271
Goodness-of-fit on F^2	1.139
Final R indexes [I>=2σ (I)]	R_1 = 0.0439, wR_2 = 0.1170
Final R indexes [all data]	R_1 = 0.0495, wR_2 = 0.1201
Largest diff. peak/hole / e Å^{-3}	1.71/-1.04

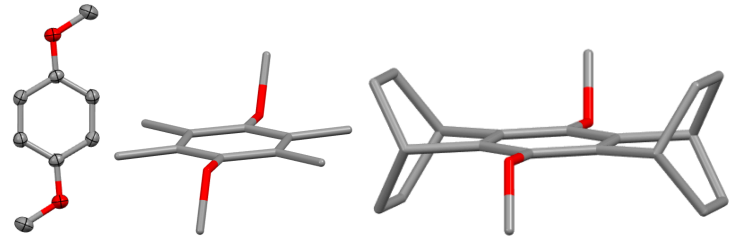

Figure S4. X-ray structures of **HE**,[7] ^{Me4}**HE**,[8] and ^{B}**HE** (left to right)[9].

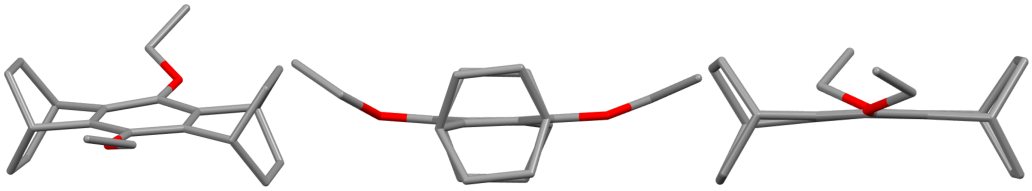

Figure S5. Different views of the ^{B}**HE**$^{+\bullet}$ ethoxy-analog X-ray structure.[10]

S3. Computational Details

Electronic structure calculations were performed with the Gaussian 09 package, revision D01.[11] For the density functional theory (DFT) calculations we used calibrated (see Ref. [12] for details) B1LYP functional[13] that contains 40% contribution of the exact exchange with 6-31G(d) basis set by Pople and co-workers.[14] Note that we[12] and others[15,16] have earlier demonstrated that alteration of the exact exchange contribution is essential to mitigate the self-interaction error[17,18] that causes artificial delocalization of spin/charge in the calculations of π-conjugated cation radicals. In this study, we found that B1LYP-40 functional provides the free energies of oxidation of various HQEs (Chart 1 in the manuscript) in slightly better agreement with the measured oxidation potentials as compared with the standard functionals M06-2X[19] and ωB97X-D[20,21] (Figures S6 and S7). For this reason as well as for the sake of consistency with our previous studies,[12] the calculations reported in this manuscript were based on the B1LYP-40 functional.

Solvent effects were included using the implicit integral equation formalism polarizable continuum model (IEF-PCM, also referred as PCM)[22-26] with the dichloromethane solvent parameters (ε = 8.93). In all DFT calculations, ultrafine Lebedev's grid was used with 99 radial shells per atom and 590 angular points in each shell. For cation radical calculations, wave function stability tests[27,28] was performed to ensure absence of solutions with lower energy. The values of $\langle S^2 \rangle$ operator after spin annihilation were confirmed to be close to the expectation value of 0.75. Unpaired spin density plots were rendered using isovalue of 0.001 a.u. Tight cutoffs on forces and atomic displacements were used to determine convergence in geometry optimization procedure. Harmonic vibrational frequency calculations were performed for the optimized structures to confirm absence of imaginary frequencies. Free energies were computed within the harmonic oscillator approximation for T = 298.15 K and P = 1 atm.

Table S10. Solution-phase (PCM) adiabatic oxidation potentials and gas-phase vertical ionization potentials, obtained by means of B1LYP-40/6-31G(d).

HQE	ΔG_{ox}, eV	*IP*, eV
HE	5.358	7.265
^{Me2}**HE**	5.144	6.931
^{Me4}**HE**	5.560	7.586
^{B}**HE**	5.429	7.394
^{M}**HE**	5.268	7.418
^{T}**HE**	5.234	7.367

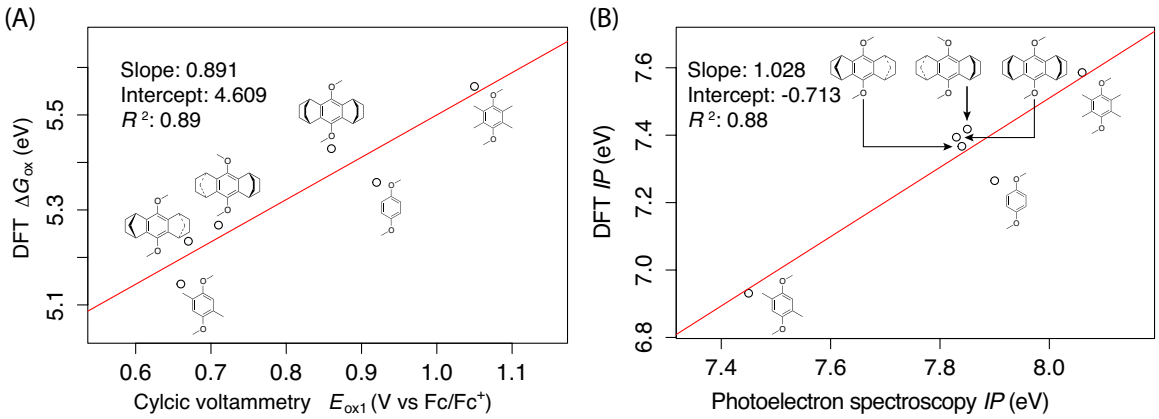

Figure S6. Comparison of the solution-phase adiabatic oxidation potentials (A) and gas-phase vertical ionization potentials (B), obtained experimentally and by means of B1LYP-40/6-31G(d).

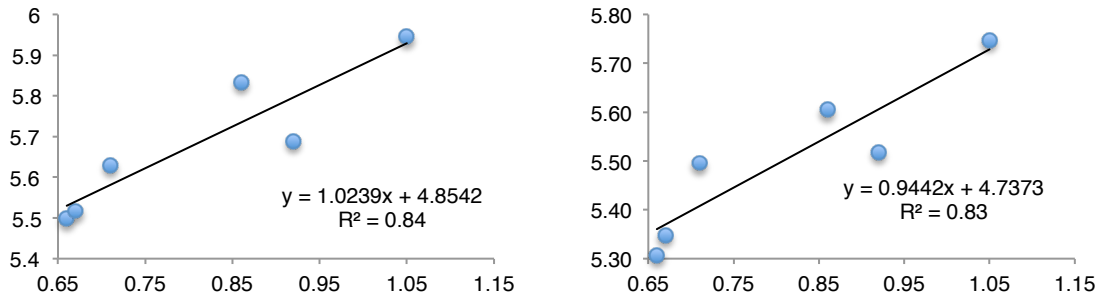

Figure S7. Comparison of the solution-phase adiabatic oxidation potentials obtained experimentally (ordinate) and by means of DFT functionals M06-2X [19] (left) and ωB97X-D [20,21] (right) using the 6-31G(d) basis set and the PCM(dichloromethane) solvation model.

S4. DFT Results

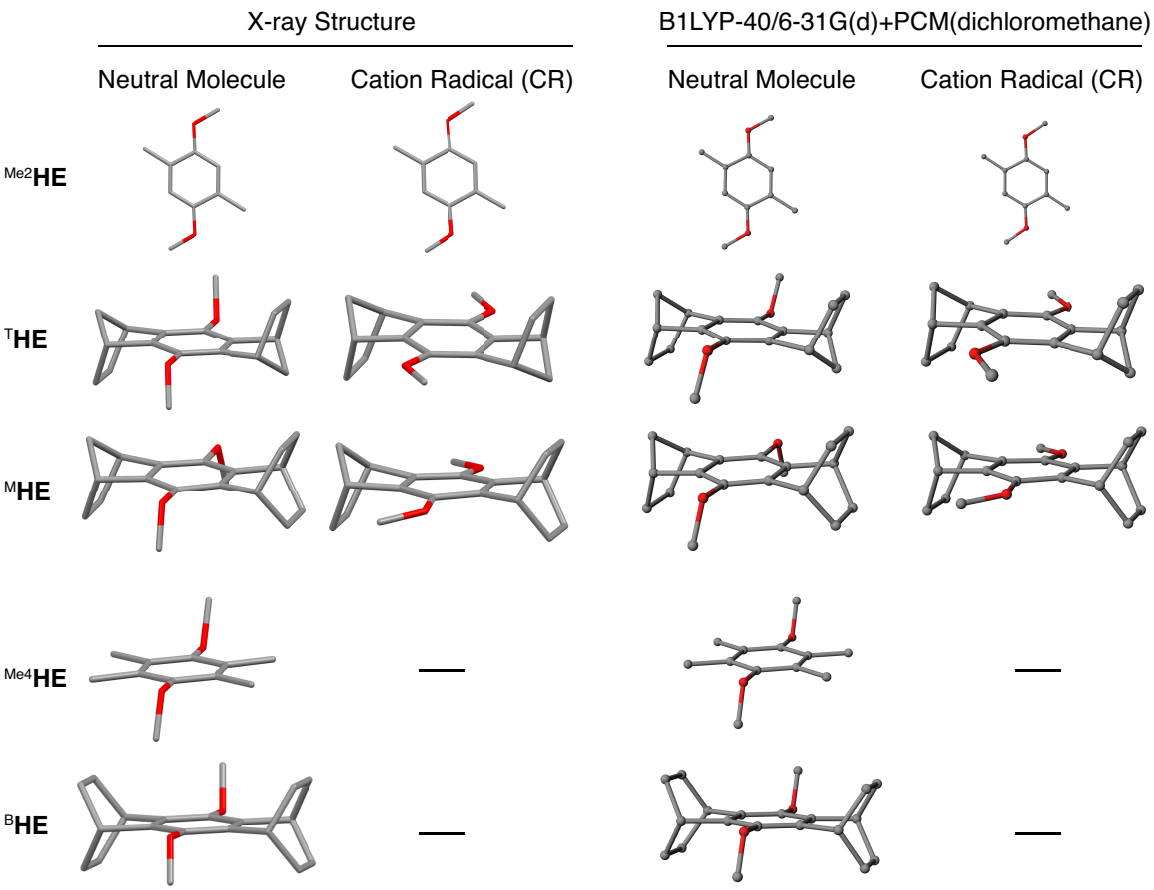

Figure S8. Comparison of the conformations of the neutral and CR HQEs obtained from X-ray crystallography vs those from the DFT calculations.

Table S11. X-ray structural parameters of neutral (N)[29,30] and cation radical (CR) ^{Me2}**HE** as well as the corresponding values obtained from the DFT calculations. Bond lengths are given in Å

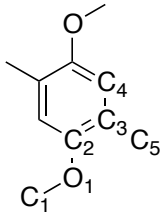

Bond	X-Ray			DFT		
	N	CR	Δ	N	CR	Δ
C1-O1	1.426	1.450	0.024	1.411	1.436	0.025
O1-C2	1.380	1.328	-0.052	1.365	1.310	-0.055
C2-C3	1.401	1.435	0.034	1.397	1.441	0.044
C3-C4	1.396	1.367	-0.029	1.392	1.368	-0.024
C4-C5	1.505	1.493	-0.012	1.504	1.495	-0.009

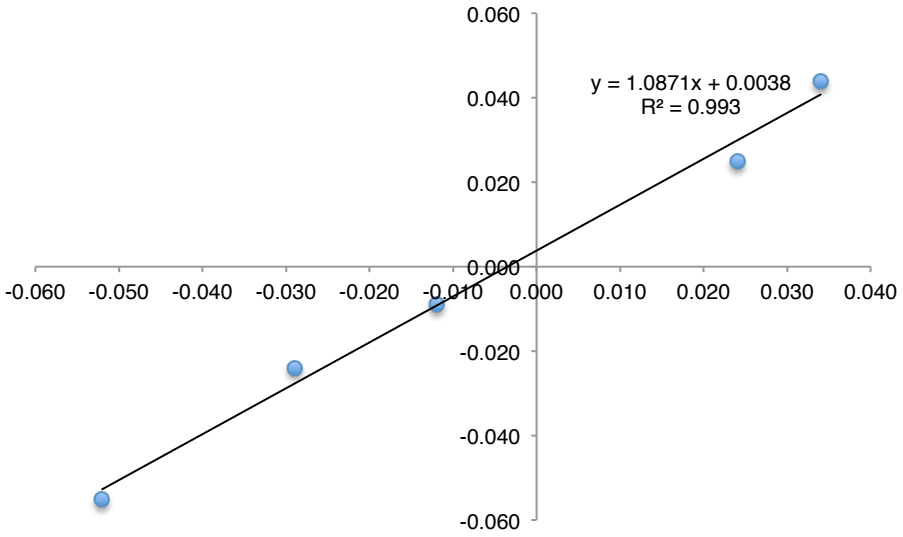

Figure S9. Comparison of the oxidation-induced bond length changes in ^{Me2}**HE** obtained by means of X-ray crystallography (abscissa) and DFT calculations (ordinate).

Table S12. X-ray structural parameters of neutral (N) [9] and cation radical (CR) [9] ^{T}**HE** as well as the corresponding values obtained from the DFT calculations. Bond lengths are given in Å

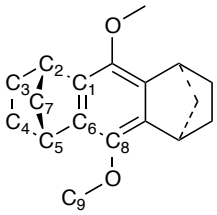

Bond	X-Ray			DFT		
	N	CR	Δ	N	CR	Δ
C1-C2	1.516	1.529	0.013	1.513	1.524	0.011
C1-C6	1.398	1.378	-0.020	1.400	1.378	-0.022
C5-C6	1.518	1.506	-0.012	1.513	1.504	-0.009
C6-C8	1.389	1.430	0.041	1.389	1.431	0.042
C8-O	1.391	1.320	-0.071	1.377	1.314	-0.063
C9-O	1.414	1.442	0.028	1.419	1.432	0.013

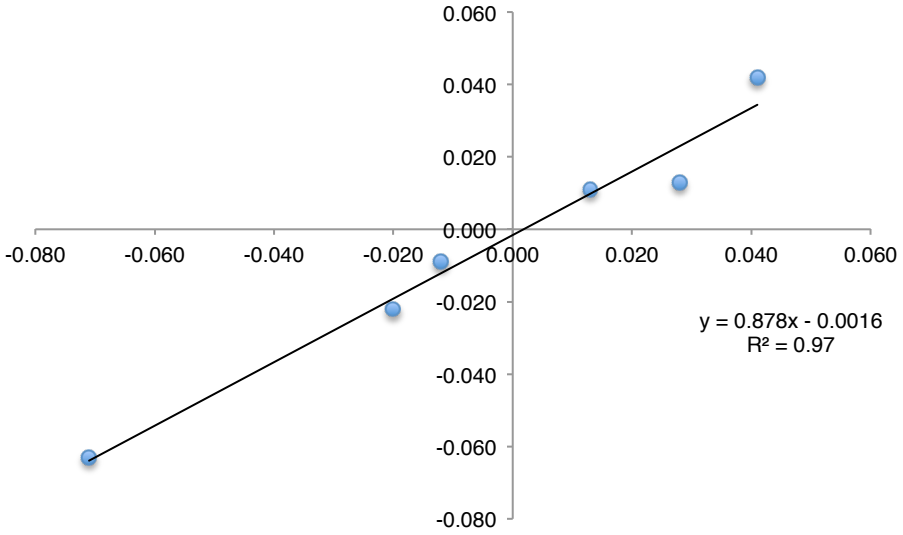

Figure S10. Comparison of the oxidation-induced bond length changes in ^{T}**HE** obtained by means of X-ray crystallography (abscissa) and DFT calculations (ordinate).

Table S13. X-ray structural parameters of neutral (N) and cation radical (CR) ^{M}**HE** as well as the corresponding values obtained from the DFT calculations. Bond lengths are given in Å

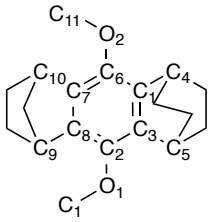

Bond	X-Ray		
	N	CR	Δ
C1-C4	1.504	1.491	-0.013
C1-C3	1.405	1.367	-0.038
C3-C5	1.504	1.503	-0.001
C2-C3	1.392	1.422	0.030
C2-O1	1.397	1.344	-0.053
C1-O1	1.422	1.436	0.014
C6-C7	1.386	1.393	0.007
C7-C8	1.406	1.388	-0.018
C8-C9	1.515	1.547	0.032
C7-C10	1.515	1.533	0.018
C6-O2	1.397	1.351	-0.046
O2-C11	1.422	1.448	0.026
C6-C1	1.392	1.396	0.004
C2-C8	1.386	1.429	0.043

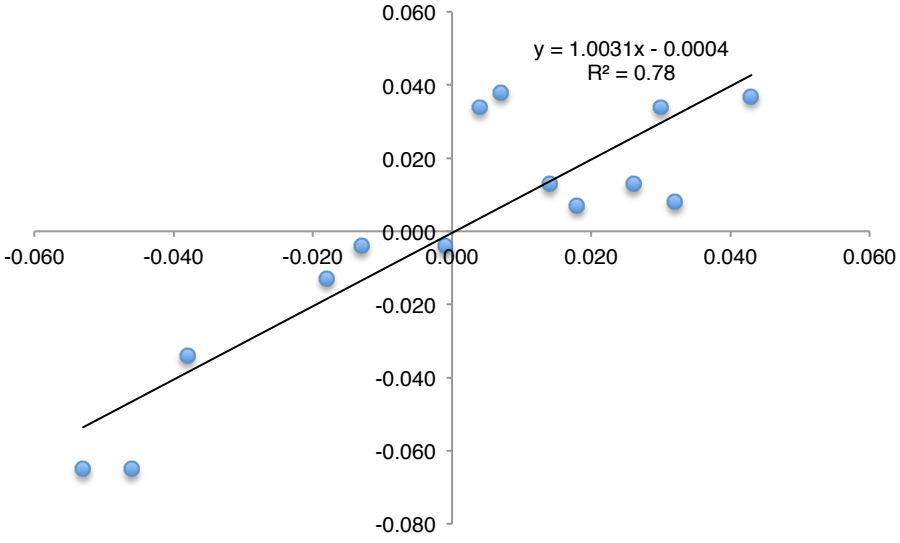

Figure S11. Comparison of the oxidation-induced bond length changes in ^{M}**HE** obtained by means of X-ray crystallography (abscissa) and DFT calculations (ordinate).

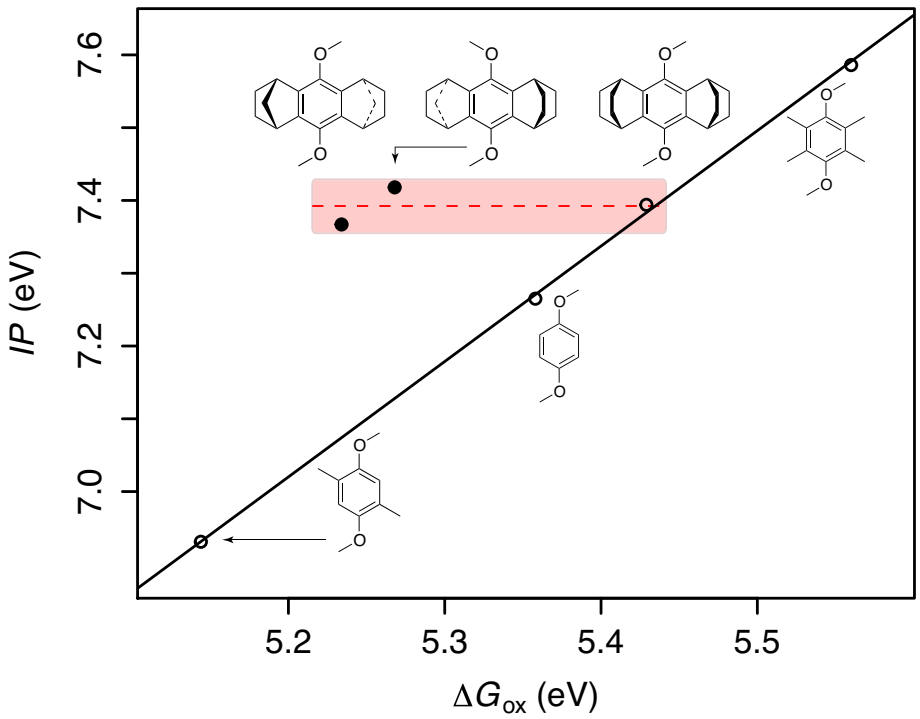

Figure S12. Calculated gas-phase ionization potentials vs solvent free energies of oxidation of HQEs obtained by means of B1LYP40/6-31G(d). The ΔG_{ox} values were computed using the polarized continuum model (PCM) with the parameters corresponding to dichloromethane.

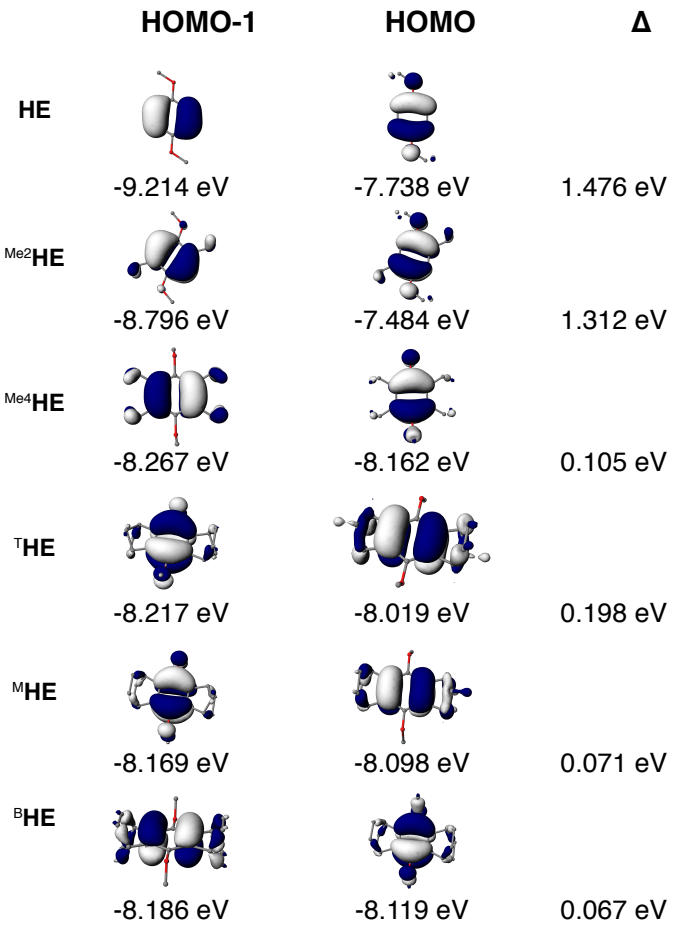

Figure S13. Isovalue (0.03 a.u.) plots and energies of the HQE HOMOs and HOMO-1 computed at the ***HF/6-31G(d)*** level of theory.

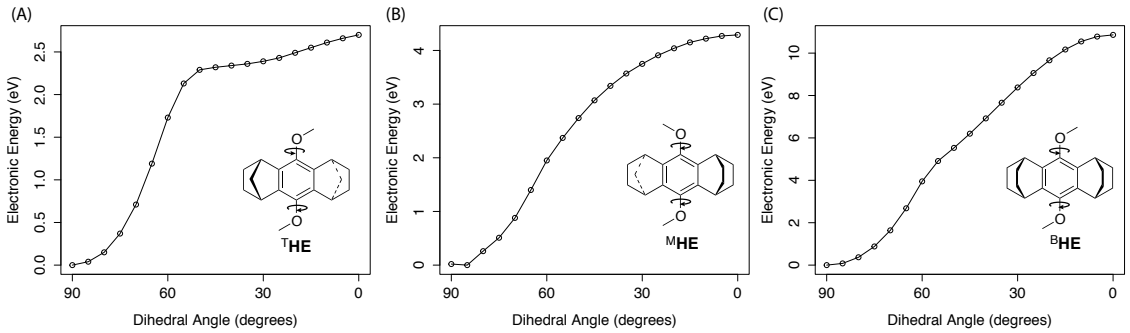

Figure S14. Electronic energies of ^{T}**HE** (A), ^{M}**HE** (B), and ^{B}**HE** (C) as function of the dihedral angle between the methoxy groups and the aromatic plane, calculated by means of B1LYP40/6-31G(d)+PCM(dichloromethane). Both methoxy groups were systematically rotated in such way that they had the same orientation toward the aromatic plane at every scan point. Other geometric parameters were optimized.

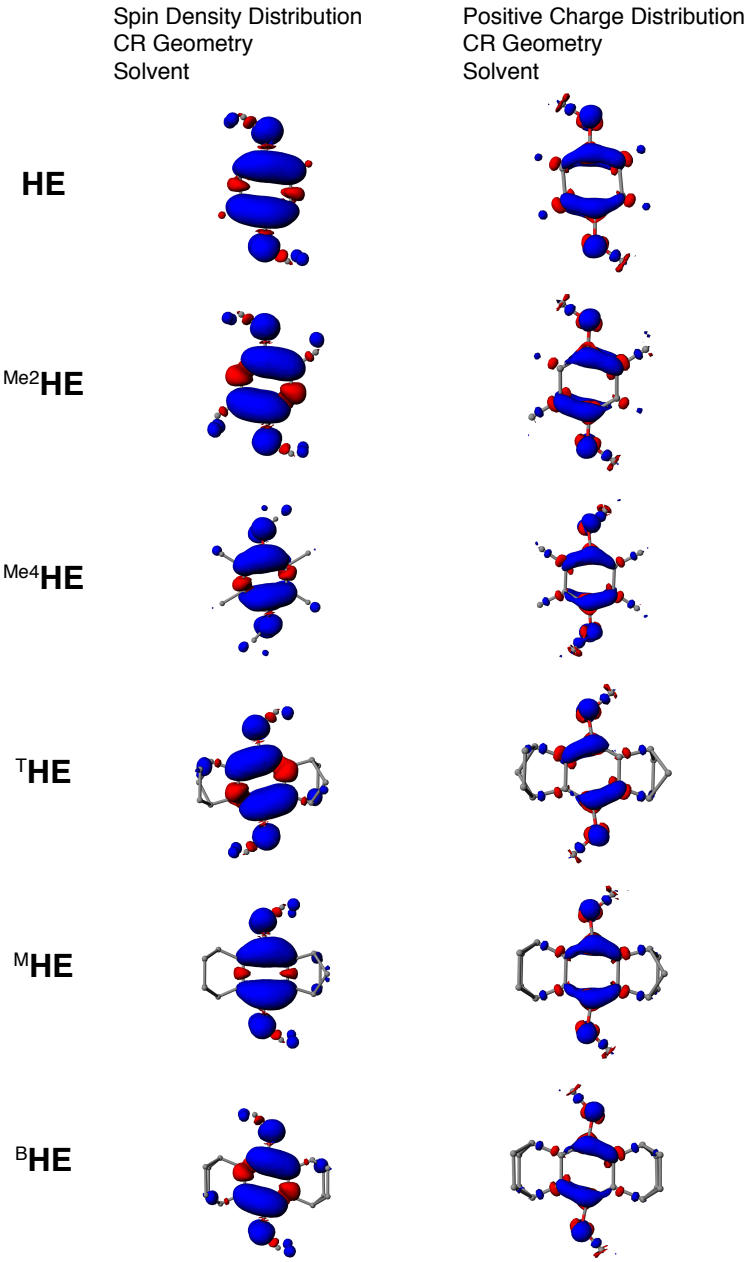

Figure S15. Comparison of the HQE CR spin density distribution (0.001 a.u.) and positive charge distribution (0.005 a.u.) isovalue plots obtained from the B1LYP-40/6-31G(d)+PCM(dichloromethane) calculations.

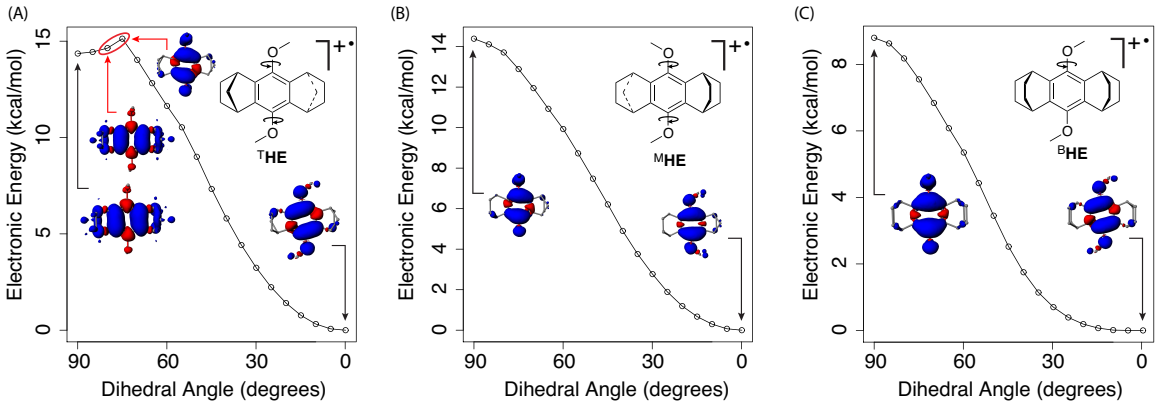

Figure S16. Electronic energies and spin density spatial distributions (0.001 a.u.) of ^{T}**HE** (A), ^{M}**HE** (B), and ^{B}**HE** (C) cation radicals as function of the CH_3-O-C_{ar1}-C_{ar2} dihedral angle [B1LYP40/6-31G(d)+PCM(CH_2Cl_2)]. This scan revealed that only ^{T}**HE** has a conformationally-induced switchover, which occurs at ~75º, whereas transformation of ^{M}**HE** from the quinoidal to bisallylic state occurs even at 90º due to the relaxation of non-fixed geometric parameters. Noteworthy, initial decrease of the dihedral angle from 90º to 75º leads to increase in energy of the CR state of ^{T}**HE**, which does not occur in the other annelated HQEs ^{M}**HE** and ^{B}**HE**. Thus, relative orientation of the methoxy groups and aromatic ring in hydroquinone ethers occurs to control the electronic structure of the corresponding cation radicals with a switchover angle of ~75º thus representing the case of electronic isomerism that is unprecedented for the aromatic cation radicals. It is also noted that the obtained spin/charge distributions at every values of the dihedral angle CH_3-O-C_{ar1}-C_{ar2} were found to be in close agreement with the shape of HOMO from the corresponding scans of neutral HQEs shown on Figure 3 in the main text.

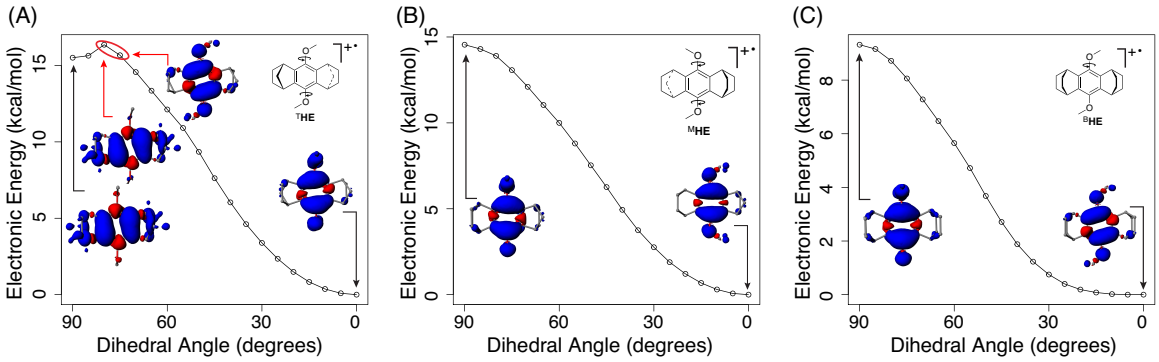

Figure S17. *Gas-phase* electronic energies and spin density spatial distributions (0.001 a.u.) of ^{T}**HE** (A), ^{M}**HE** (B), and ^{B}**HE** (C) cation radicals as function of the dihedral angle between the methoxy groups and the aromatic plane, calculated by means of B1LYP40/6-31G(d) without solvent modeling. Both methoxy groups were systematically rotated in such way that they had the same orientation toward the aromatic plane at every scan point. Other geometric parameters were optimized.

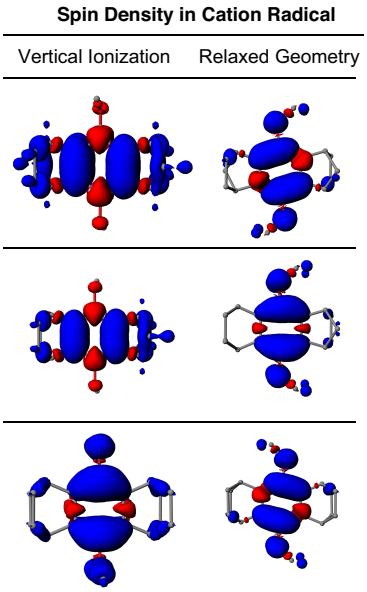

Figure S18. Isovalue plots of the full spin density spatial distributions (0.001 a.u.) in the HQE CRs [B1LYP40/6-31G(d)+PCM(CH_2Cl_2)].

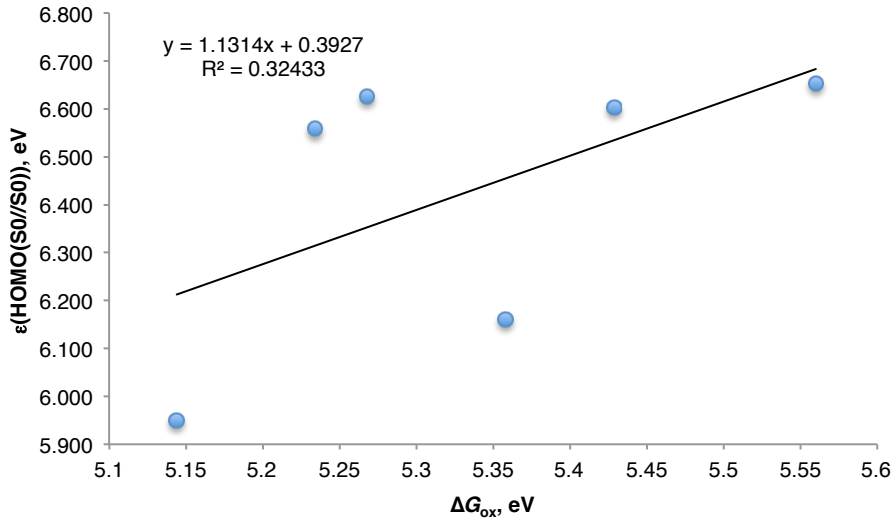

Figure S19. Relationship between ΔG_{ox} vs HOMOs of the HQEs from Chart 1, denoted as HOMO(S0//S0) [B1LYP40/6-31G(d)+PCM(CH_2Cl_2)].

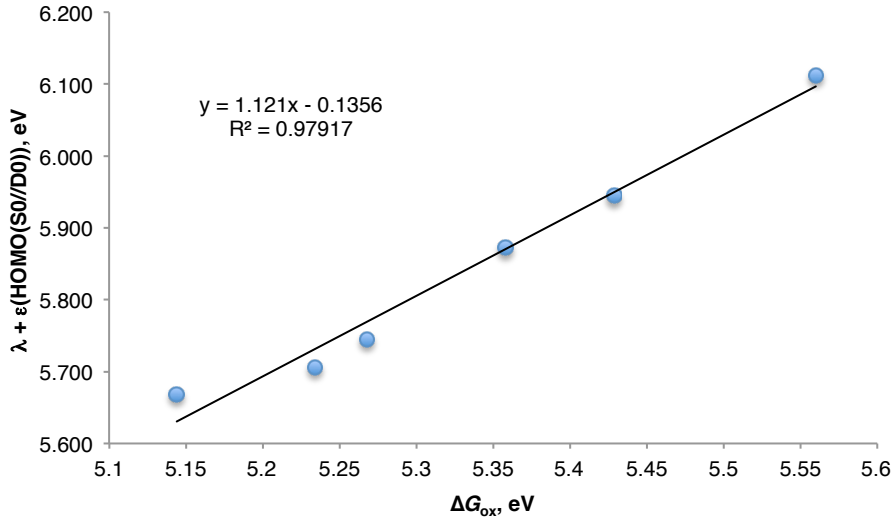

Figure S20. Relationship between ΔG_{ox} vs HOMOs of neutral HQEs that were structurally reorganized upon 1-electron oxidation [denoted as HOMO(S0//D0)] with the structural reorganization energy taken into account [$\lambda = E$(S0//D0) – E(S0//S0)], B1LYP40/6-31G(d)+PCM(CH_2Cl_2).

S5. References

(1) Navale, T. S.; Zhai, L.; Lindeman, S. V.; Rathore, R. Octamethoxydibenzochrysene: Isolation and X-ray Crystallographic Characterization of a Twisted Polyaromatic Cation Radical. *Chem. Commun.* **2009,** 2857-2859.

(2) Banerjee, M.; Vyas, V. S.; Lindeman, S. V.; Rathore, R. Isolation and X-ray Structural Characterization of Tetraisopropylpyrene Cation Radical. *Chem. Commun.* **2008,** 1889-1891.

(3) Chebny, V. J.; Navale, T. S.; Shukla, R.; Lindeman, S. V.; Rathore, R. X-ray Structural Characterization of Charge Delocalization onto the Three Equivalent Benzenoid Rings in Hexamethoxytriptycene Cation Radical. *Org. Lett.* **2009,** *11,* 2253-2256.

(4) Navale, T. S.; Thakur, K.; Vyas, V. S.; Wadumethrige, S. H.; Shukla, R.; Lindeman, S. V.; Rathore, R. Charge Delocalization in Self-assembled Mixed-valence Aromatic Cation Radicals. *Langmuir* **2012,** *28,* 71-83.

(5) Shukla, R.; Wadumethrige, S. H.; Lindeman, S. V.; Rathore, R. Synthesis, Electronic Properties, and X-ray Structural Characterization of Tetrarylbenzo[1,2-b:4,5-b']difuran Cation Radicals. *Org. Lett.* **2008,** *10,* 3587-3590.

(6) Chebny, V. J.; Shukla, R.; Lindeman, S. V.; Rathore, R. Molecular Actuator: Redox-controlled Clam-like Motion in a Bichromophoric Electron Donor. *Org. Lett.* **2009,** *11,* 1939-1942.

(7) Iuliucci, R.; Hoop, C. L.; Arif, A. M.; Harper, J. K.; Pugmire, R. J.; Grant, D. M. Redetermination of 1,4-dimethoxy-benzene. *Acta. Crystallogr. Sect. E Struct. Rep. Online* **2009,** *65,* o251.

(8) Wieczorek, M. W.; Bokii, N. G.; Struchkov, Y. T. Roczniki Chemii. *Roczniki Chemii* **1975,** *49,* 1737.

(9) Rathore, R.; Kochi, J. K. Isolation of Novel Radical Cations from Hydroquinone Ethers. Conformational Transition of the Methoxy Group upon Electron Transfer. *J. Org. Chem.* **1995,** *60,* 4399-4411.

(10) Rosokha, S. V.; Kochi, J. K. Mechanism of Inner-sphere Electron Transfer via Charge-transfer (Precursor) Complexes. Redox Energetics of Aromatic Donors with the Nitrosonium Acceptor. *J. Am. Chem. Soc.* **2001,** *123,* 8985-8999.

(11) Frisch, M. J.; Trucks, G. W.; Schlegel, H. B.; Scuseria, G. E.; Robb, M. A.; Cheeseman, J. R.; Scalmani, G.; Barone, V.; Mennucci, B.; Petersson, G. A.; Nakatsuji, H.; Caricato, M.; Li, X.; Hratchian, H. P.; Izmaylov, A. F.; Bloino, J.; Zheng, G.; Sonnenberg, J. L.; Hada, M.; Ehara, M.; Toyota, K.; Fukuda, R.; Hasegawa, J.; Ishida, M.; Nakajima, T.; Honda, Y.; Kitao, O.; Nakai, H.; Vreven, T.; Montgomery, J. A.; Peralta, J. E.; Ogliaro, F.; Bearpark, M.; Heyd, J. J.; Brothers, E.; Kudin, K. N.; Staroverov, V. N.; Kobayashi, R.; Normand, J.; Raghavachari, K.; Rendell, A.; Burant, J. C.; Iyengar, S. S.; Tomasi, J.; Cossi, M.; Rega, N.; Millam, J. M.; Klene, M.; Knox, J. E.; Cross, J. B.; Bakken, V.; Adamo, C.; Jaramillo, J.; Gomperts, R.; Stratmann, R. E.; Yazyev, O.; Austin, A. J.; Cammi, R.; Pomelli, C.; Ochterski, J. W.; Martin, R. L.; Morokuma, K.; Zakrzewski, V. G.; Voth, G. A.; Salvador, P.; Dannenberg, J. J.; Dapprich, S.; Daniels, A. D.; Farkas; Foresman, J. B.; Ortiz, J. V.; Cioslowski, J.; Fox, D. J. Gaussian, Inc., Wallingford CT, 2009.

(12) Talipov, M. R.; Boddeda, A.; Timerghazin, Q. K.; Rathore, R. Key Role of End-Capping Groups in Optoelectronic Properties of Poly-p-phenylene Cation Radicals. *J. Phys. Chem. C* **2014,** *118,* 21400-21408.

(13) Adamo, C.; Barone, V. Toward Reliable Adiabatic Connection Models Free from Adjustable Parameters. *Chem. Phys. Lett.* **1997,** *274,* 242-250.

(14) Hehre, W. J.; Ditchfield, R.; Pople, J. A. Self-consistent Molecular Orbital Methods. XII. Further Extensions of Gaussian-type Basis Sets for Use in Molecular Orbital Studies of Organic Molecules. *J. Chem. Phys.* **1972,** *56,* 2257-2261.

(15) Renz, M.; Theilacker, K.; Lambert, C.; Kaupp, M. A Reliable Quantum-chemical Protocol for the Characterization of Organic Mixed-valence Compounds. *J. Am. Chem. Soc.* **2009,** *131,* 16292-16302.

(16) Renz, M.; Kess, M.; Diedenhofen, M.; Klamt, A.; Kaupp, M. Reliable Quantum Chemical Prediction of the Localized/Delocalized Character of Organic Mixed-Valence

Radical Anions. From Continuum Solvent Models to Direct-COSMO-RS. *J. Chem. Theory. Comput.* **2012,** *8,* 4189-4203.

(17) Cohen, A. J.; Mori-Sánchez, P.; Yang, W. Insights into Current Limitations of Density Functional Theory. *Science* **2008,** *321,* 792-794.

(18) Cohen, A. J.; Mori-Sánchez, P.; Yang, W. Challenges for Density Functional Theory. *Chem. Rev.* **2011,** *112,* 289-320.

(19) Zhao, Y.; Truhlar, D. G. The M06 Suite of Density Functionals for Main Group Thermochemistry, Thermochemical Kinetics, Noncovalent Interactions, Excited States, and Transition Elements: Two New Functionals and Systematic Testing of Four M06-class Functionals and 12 Other Functionals. *Theor. Chem. Acc.* **2008,** *120,* 215-241.

(20) Chai, J. -D.; Head-Gordon, M. Systematic Optimization of Long-range Corrected Hybrid Density Functionals. *J. Chem. Phys.* **2008,** *128,* 084106.

(21) Chai, J.-D.; Head-Gordon, M. Long-range Corrected Hybrid Density Functionals with Damped Atom-atom Dispersion Corrections. *Phys. Chem. Chem. Phys.* **2008,** *10,* 6615-6620.

(22) Miertus, S.; Scrocco, E.; Tomasi, J. Electrostatic Interaction of a Solute with a Continuum. A Direct Utilization of ab initio Molecular Potentials for the Prevision of Solvent Effects. *Chem. Phys.* **1981,** *55,* 117-129.

(23) Cances, M. T.; Mennucci, V.; Tomasi, J. A New Integral Equation Formalism for the Polarizable Continuum Model: Theoretical Background and Applications to Isotropic and Anisotropic Dielectrics. *J. Chem. Phys.* **1997,** *107,* 3032-3041.

(24) Cossi, M.; Barone, V.; Mennucci, V.; Tomasi, J. Ab Initio Study of Ionic Solutions by a Polarizable Continuum Dielectric Model. *Chem. Phys. Lett.* **1998,** *286,* 253-260.

(25) Tomasi, J.; Mennucci, B.; Cammi, R. Quantum Mechanical Continuum Solvation Models. *Chem. Rev.* **2005,** *105,* 2999-3093.

(26) Ribeiro, R. F.; Marenich, A. V.; Cramer, C. J.; Truhlar, D. G. Use of Solution-Phase Vibrational Frequencies in Continuum Models for the Free Energy of Solvation. *J. Phys. Chem. B.* **2011,** *115,* 14556-14562.

(27) Seeger, R.; Pople, J. A. Self-consistent Molecular Orbital Methods. XVIII. Constraints and Stability in Hartree–Fock theory. *J. Chem. Phys.* **1977,** *66,* 3045-3050.

(28) Bauernschmitt, R.; Ahlrichs, R. Stability Analysis for Solutions of the Closed Shell Kohn-Sham equation. *J. Chem. Phys.* **1996,** *104,* 9047-9052.

(29) Sun, D.; Lindeman, S. V.; Rathore, R.; Kochi, J. K. Intramolecular (Electron) Delocalization Between Aromatic Donors and their Tethered Cation-radicals. Application of Electrochemical and Structural Probes. *J. Chem. Soc. Perk. T. 2.* **2001,** 1585-1594.

(30) Lindeman, S. V.; Rosokha, S. V.; Sun, D.; Kochi, J. K. X-ray Structure Analysis and the Intervalent Electron Transfer in Organic Mixed-valence Crystals with Bridged Aromatic Cation Radicals. *J. Am. Chem. Soc.* **2002,** *124,* 843-855.